Clim Dyn
DOI 10.1007/s00382-014-2377-0

Robustness of the modes of Indo-Pacific sea level variability

Leela M. Frankcombe · Shayne McGregor · Matthew H. England

Received: 29 June 2014 / Accepted: 13 October 2014

Abstract This study evaluates the influence of various climate modes on sea level. The altimetry record has excellent spatial coverage but the limited length becomes an issue when evaluating low frequency variability in the presence of a trend. We use altimetry along with two ocean models to study how the relationship between sea surface height (SSH) in the Indian and Pacific Oceans and four climate modes [the Pacific Decadal Oscillation (PDO), the El Niño–Southern Oscillation, the Indian Ocean Dipole and the Southern Annular Mode] depends on the length of the time series. For low frequency variability such as the PDO, a time series on the order of 50 years in length is required to separate variability from the trend. Using shorter time series results in aliasing of the SSH trend and low frequency variability, which has implications for ascertaining the role of the PDO in the SSH trends. We find that the regression of SSH on to the PDO during the altimetry period, which is thought to have been responsible for a large fraction of the recent western Pacific SSH trend, is not representative of the SSH–PDO relationship in the longer-term record.

Keywords Sea level variability · Decadal variability · Multidecadal variability · Pacific Decadal Oscillation · Indian Ocean Dipole · El Nino Southern Oscillation

L. M. Frankcombe (✉) · S. McGregor · M. H. England
ARC Centre of Excellence for Climate System Science and Climate Change Research Centre, University of New South Wales, Sydney, NSW, Australia
e-mail: l.frankcombe@unsw.edu.au

1 Introduction

Reliable projections of future sea level are vital for coastal communities. Regional deviations from global mean sea level rise are caused primarily by spatial patterns in the various components of sea level change (e.g. melting land ice, thermal expansion, and so on; see Slangen et al. 2012; Perrette et al. 2013; Church et al. 2013) and by wind anomalies associated for example with various climate modes. Whether and how these climate modes might change in the future is an important question, however, understanding their current signature in sea level is the first step.

Sea level is observed using both satellite altimeters and tide gauges. Altimetry provides excellent spatial coverage but the time series is of limited length, meaning that interannual to decadal variability remains difficult to resolve. Longer records from tide gauges are available, however, these lack spatial resolution as they measure SSH only at a few points along the coastline. The sparsity of tide gauges along with their uneven spatial distribution makes it difficult to study the spatial patterns of variability in both the empty interiors of the ocean and along the large sections of coastlines where tide gauge records are short or altogether absent. This problem is particularly apparent in the southern hemisphere, where long tide gauge records are extremely sparse. Statistical reconstructions using altimetry and tide gauges are of limited use for studying low frequency variability since these time scales are not sampled in the short satellite record (Ray and Douglas 2011; Meyssignac et al. 2012b; Calafat et al. 2014).

The problem of extracting low frequency variability from short time series is exacerbated by the presence of the trend due to anthropogenic climate change [and vice versa, see Cazenave et al. (2014), for example]. Separating the forced trend from the natural variability is not as simple as

Published online: 22 October 2014

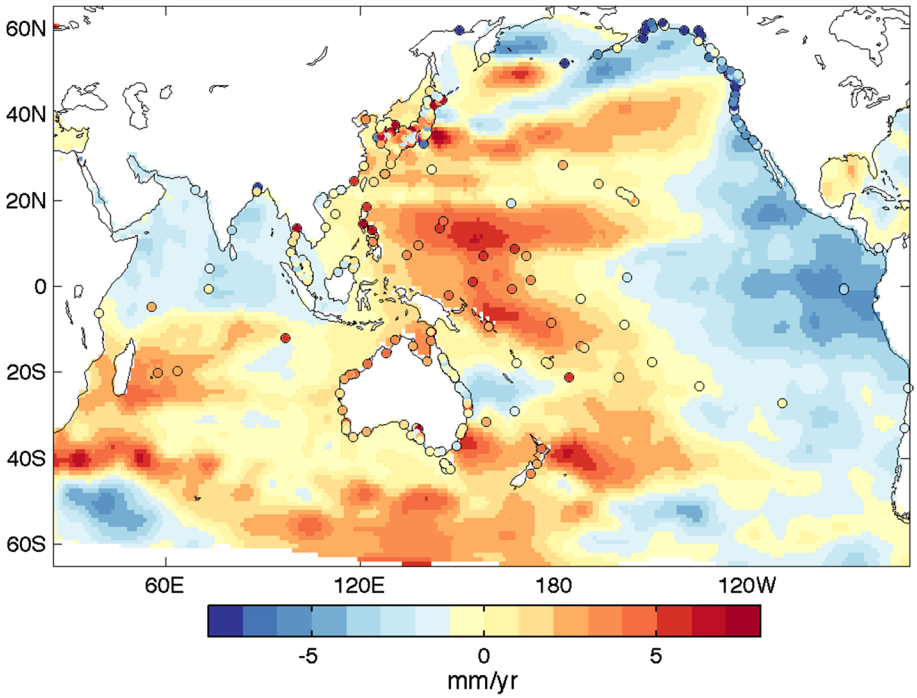

Fig. 1 Linear trend in SSH (in mm/year) from altimetry (*contours*) and tide gauges (*circles*) over the period 1993–2007

subtracting a linear trend (Mann et al. 2014) or even the long term global average since the trend is not necessarily linear or spatially uniform. In addition, these procedures to remove the anthropogenic trend may also remove part of the low frequency variability in which we are interested, particularly in relatively short records. This difficulty in separating the trend and low frequency variability is of particular importance in the tropical Pacific for example, where SSH has displayed extremely large positive trends (shown in Fig. 1) in the last few decades caused by a combination of global sea level rise, variations in the strength of the trade winds and variations in climate modes (Meyssignac et al. 2012a; McGregor et al. 2012a; Merrifield et al. 2012; England et al. 2014). Timmermann et al. (2010) and Qiu and Chen (2012) found that recent rapid sea level variations in this region are caused by the thermosteric effect of redistribution of upper ocean water masses due to changes in the wind field.

Sea level variability in several other regions of the Pacific have also been investigated in detail. Qiu and Chen (2006) studied the extra-tropical south Pacific and linked sea level increases there to wind-driven baroclinic Rossby waves. Roemmich et al. (2007) further explained this increase as thermosteric and associated the wind changes responsible with the intensification of the Southern Annular Mode. Many studies have connected variability in the Indo-Pacific with ENSO and/or the PDO. Feng et al. (2004) correlated Fremantle sea level with the PDO while Cai et al. (2005) looked at the propagation of ENSO signals along the north-west Australian coast. Earlier, Enfield and Allen (1980) studied the propagation of SSH signals along the Pacific coast of the Americas and associated these with ENSO. More recently, Zhang and Church (2012) looked at the relationship between interannual and decadal variability of SSH in the Pacific and indices of ENSO and the PDO. They found that the high rate of sea level rise in the western tropical Pacific over the altimeter era has a significant component associated with the PDO.

In this paper we study how interannual to decadal scale variability in SSH in the Indian and Pacific Oceans is related to the various climate modes which are dominant in the region, namely the Pacific Decadal Oscillation/Interdecadal Pacific Oscillation (PDO/IPO), the El Niño/Southern Oscillation (ENSO), the Indian Ocean Dipole (IOD) and the Southern Annular Mode (SAM). To avoid the limitations imposed by the short length of the altimetry record and the sparse spatial coverage of the tide gauges we also use data from two different ocean models, each forced with a different wind product. The use of two models allows us to test how robust the relationships between SSH and the various climate modes are to changes in the timing and length of the interval under consideration, as well as to the impact of using different wind forcing products.

2 Data and methods

We use monthly averages of the combined TOPEX/Poseidon, Jason-1 and Jason-2/OSTM sea level fields obtained from the sea level data holdings of the Commonwealth Scientific and Industrial Research Organisation

(http://www.cmar.csiro.au/sealevel/sl_data_cmar.html, data from January 1993 to December 2012). Data is on a $1^\circ \times 1^\circ$ grid and the inverse barometer (IB) and glacial isostatic adjustment (GIA) corrections have been applied. Tide gauges in the Indian and Pacific Oceans were obtained from the Permanent Service for Mean Sea Level (PSMSL; http://www.psmsl.org/data/). The signals were corrected for the IB effect using pressures from HadSLP2 (Allan and Ansell 2006) and for the GIA effect using the ICE-5G model (Peltier 2004). Tide gauges were included if they had data for more than two thirds of months in each time window. In order to focus on the variability of SSH, global mean sea level has been removed from both altimetry and the tide gauges using the time series of Church and White (2011).

For comparison with the observations we use output from two models. The first is the 1/4° Australian Community Climate and Earth System Simulator-Ocean-Eddy Permitting (ACCESS-OEP) global ocean-sea ice model (Frankcombe et al. 2013; Spence et al. 2014) which is based on the Modular Ocean Model version 5 (MOM5; Griffies 2012) with the ocean–ice configuration from the GFDL CM2.5 climate model (Delworth et al. 2012). The ocean model is forced with the CORE-IAF_v2 data (Griffies et al. 2009, 2014) which uses NCEP winds. This simulation covers the period 1947 to 2007 and will be referred to here as MOM0.25. The second model is the Simple Ocean Data Assimilation version 2.1.6 (SODA; Carton and Giese 2008; Czeschel et al. 2011), which uses ERA-40 winds until 2001 and ERA-interim winds thereafter. The model (which will be referred to here as SODA) assimilates hydrographic data but not satellite altimetry and covers the period 1958 to 2008. In order to compare SODA and MOM0.25 we will use the period 1958 to 2007, while for comparisons to altimetry we will use the period 1993 to 2007.

The long-term mean seasonal cycle was removed from both observations and model data and all time series were smoothed using a 5 month running mean. We use data covering the Indian and Pacific Oceans, from 65°S to 65°N and 25°E to 70°W.

Indices of four climate modes (PDO, ENSO, IOD and SAM) are used. The PDO index is defined as the leading principal component of monthly SST in the North Pacific (poleward of 20°N) with global average anomalies removed (Mantua et al. 1997). The spatial pattern of the PDO is calculated over the period 1900–1993 rather than individually over each shorter period investigated here to allow comparisons between periods. Using the Interdecadal Pacific Oscillation (IPO; Power et al. 1999) in place of the PDO does not change the results as they are both qualitatively similar (Folland et al. 2002). ENSO is represented by two timeseries, following Stuecker et al. (2013). The first ENSO index (ENSO_1) is the Multivariate ENSO Index (MEI) of Wolter and Timlin (2011), smoothed as described below. The second ENSO index (ENSO_2) is constructed by multiplying ENSO_1 by $\cos(\omega_{at} - \theta)$ where ω_a is the angular frequency of the annual cycle and θ is a 1 month phase shift. This second ENSO index describes the nonlinear atmospheric response to SST anomalies associated with the combination of ENSO and the annual cycle (Stuecker et al. 2013). Using various other ENSO indices such as Niño3.4 or the Southern Oscillation Index (SOI) in place of the MEI did not significantly affect the results. The IOD is represented by the Dipole Mode Index (Saji et al. 1999) calculated from the HadISST dataset. The SAM index is calculated as described in Marshall (2003).

The PDO can be considered, to first order, to be a low pass filter of ENSO variability (Kleeman et al. 1999; Newman et al. 2003). As we are interested in separating the two time scales, the time series are smoothed following the method of Zhang and Church (2012). Namely, the high frequency variability is isolated in the ENSO indices by smoothing with a 5 month running mean and then subtracting the low frequency component which is estimated by smoothing the indices with successive 25 and 37 month running means. The PDO index has the high frequency component removed by smoothing with successive 25 and 37 month running means. This separates the high and low frequency components as far as possible. For simplicity the smoothed indices will be referred to as ENSO for the short time scales and PDO for the long time scales. The IOD and SAM indices are both smoothed with a 5 month running mean. All indices are normalised by their standard deviation and are plotted in Fig. 2a. Correlations between the various indices are listed in Table 1.

To identify the relationships between SSH and the (smoothed) climate indices we follow the method of Zhang and Church (2012). The multiple variable linear regression between SSH and the indices is calculated as follows:

$$\begin{aligned}\mathrm{SSHA} = {} & a_0 + a_1 \mathrm{t} + a_2 \mathrm{PDO} + a_3 \mathrm{ENSO}_1 \\ & + a_4 \mathrm{ENSO}_2 + a_5 \mathrm{IOD} + a_6 \mathrm{SAM} + \epsilon \end{aligned} \quad (1)$$

where a_n are the regression coefficients, t is a residual linear trend and ϵ is the residual variability. The goodness of fit of the regression is measured by the R^2 value which is defined as the amount of variance explained by the regression divided by the total variance of the original time series. The pattern of regression coefficients a_n calculated by this method may be considered to be the linear part of the pattern of SSH variability associated with each climate index. The residual linear trend term t is included to capture the component of the linear trend not explained by the climate indices. It may include trends due to natural or anthropogenically induced components. Care must be taken when investigating the role of the defined climate indices in the trend calculated over short window lengths as parts of the trend may be artificially attributed to a low frequency climate mode (i.e. low frequency variability aliased as a trend, see Fig. 2b). The

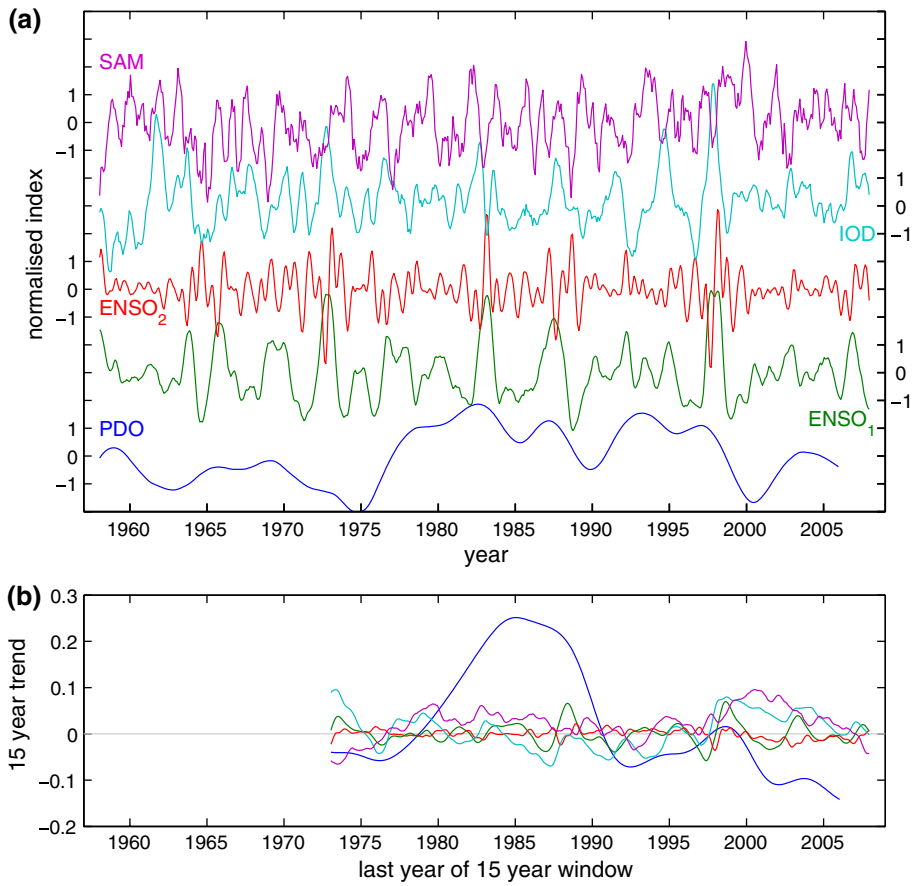

Fig. 2 **a** Normalised timeseries of the climate modes used in the regression calculations: the Pacific Decadal Oscillation (*PDO*, in *blue*), the first ENSO index ($ENSO_1$, in *green*), the second ENSO index ($ENSO_2$, in *red*), the Indian Ocean Dipole (*IOD*, in *cyan*) and the Southern Annular Mode (*SAM*, in *magenta*). **b** 15-year trends of the indices in (**a**), plotted against the last year of the 15-year window

Table 1 Correlations between the climate indices from 1958 to 2007

Indices	PDO	$ENSO_1$	$ENSO_2$	IOD	SAM
PDO	**1**	–	–	–	–
$ENSO_1$	**0.09**	**1**	–	–	–
$ENSO_2$	0.01	0.01	**1**	–	–
IOD	**−0.10**	**0.40**	**−0.29**	**1**	–
SAM	**0.12**	**−0.11**	**−0.18**	**0.14**	**1**

Values which are significant at the 95 % level are indicated in bold

residual ϵ is SSH variability that is not explained by the multiple variable linear regression and may be due to stochastic processes, modes of variability not included in our calculations, nonlinearities in external forcing (both natural and anthropogenic), or nonlinearities in the relationships between SSH and the various climate indices that are included.

3 Results

3.1 Altimetry

Figure 3 shows the coefficients for a multiple variable linear regression using a residual linear trend, the PDO index, the two ENSO indices, the IOD index and the SAM index for altimetry as well as tide gauges over the 15-year period 1993–2007.

The pattern of SSH regressed on to the PDO (Fig. 3b) has high sea level in the central and eastern tropical Pacific, extending in a band along the coast of North America (and to a lesser extent along the coast of South America). There is low sea level in the central north Pacific and the western tropical Pacific, extending into the eastern Indian Ocean and along the coast of Western Australia. There are also significant regressions in the Southern Ocean. Comparing this PDO-related SSH pattern to the linear trend calculated directly from altimetry (Fig. 1) we can see that the linear altimetry trend resembles the negative PDO-related SSH pattern, particularly in the Pacific. This negative PDO-related SSH pattern corresponds to the negative trend that has been observed in the PDO during the altimetry period (see Fig. 2b). The part of the linear altimetry trend which is not explained by the trend in the PDO index appears as the residual trend in Fig. 3a.

The SSH pattern regressed on to the first ENSO index (Fig. 3c) resembles the PDO-related SSH pattern in the tropics, with the signals decaying rapidly away from the equator. Very narrow bands of high regression coefficients occur along the coast of the Americas. The PDO and first

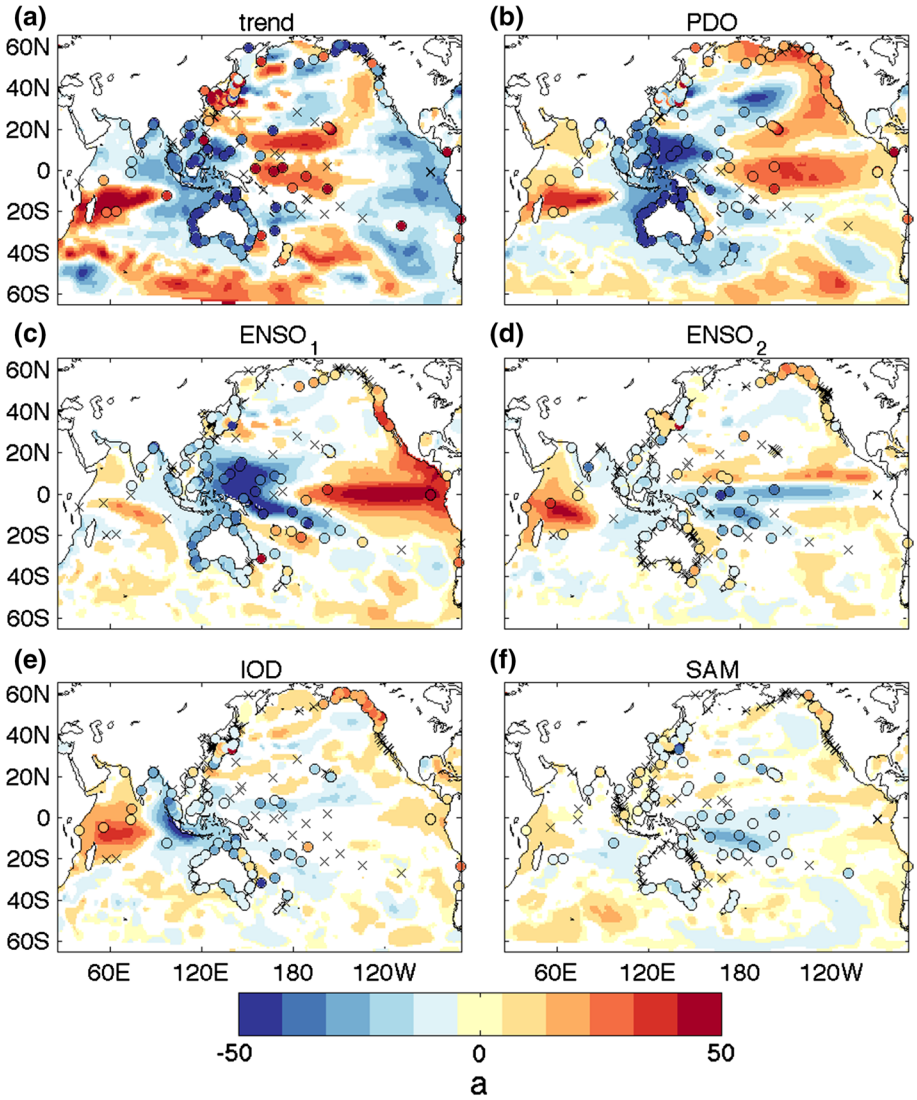

Fig. 3 Regression patterns for SSH from altimetry from 1993 to 2007 related to **a** the residual trend, **b** the PDO, **c** and **d** two ENSO indices, **e** the IOD and **f** the SAM. Regression coefficients which are not significantly different from zero (at the 95 % level) are not shown. *Coloured circles* indicate significant regression coefficients calculated for tide gauges. Wherever tide gauge data is available but the coefficients are not significant a *cross* symbol is used

ENSO-related SSH patterns are similar to those shown by Zhang and Church (2012) for the Pacific. The second ENSO-related SSH pattern (Fig. 3d) is similar to that found by Widlansky et al. (2014) for the western tropical Pacific, with significance along the equator and in the South Pacific Convergence Zone. The spatial structures of the two ENSO patterns are consistent with the 'east-west tilting mode' and the 'recharge mode' (Meinen and McPhaden 2000; McGregor et al. 2012b). The IOD-related SSH pattern (Fig. 3e) has the largest amplitude in the Indian Ocean with a sea level high in the western Indian Ocean and a sea level low along the coast of Java and Sumatra. The IOD-related SSH pattern also has significant values in the tropical Pacific, as do the ENSO-related SSH patterns in the Indian Ocean, indicating that these indices are not independent over the short observational record (see also Table 1). The SAM-related SSH pattern has significant values in the equatorial Pacific, which may be related to the influence of the tropics on the SAM (Ding et al. 2012), as well as significant values in the Southern Ocean (although altimetry only extends to 60°S).

Together the PDO, $ENSO_1$, $ENSO_2$, IOD and SAM indices have an R^2 of 47.28 %, meaning that they explain 47.28 % of the SSH variability over the domain shown (65° –65°N, 25°E–70°W). The improvement in R^2 (of 7.06 %) by including $ENSO_2$, the IOD and SAM over PDO and $ENSO_1$ alone is shown in Fig. 4.

Table 2 lists R^2 values when different indices are included in the regression calculation, giving an indication of the independence of the indices. For example, $ENSO_1$ has an R^2 value of 13.80 on its own, $ENSO_2$ has a value of 1.99 while both together have a value of 15.58, illustrating that the two are largely independent. The IOD, on the other hand, has an R^2 value of 6.13 on its own, but only increases to an R^2 value of 18.73 when combined with the two ENSO indices, showing that about half of the SSH variability attributed to the IOD could also be explained by

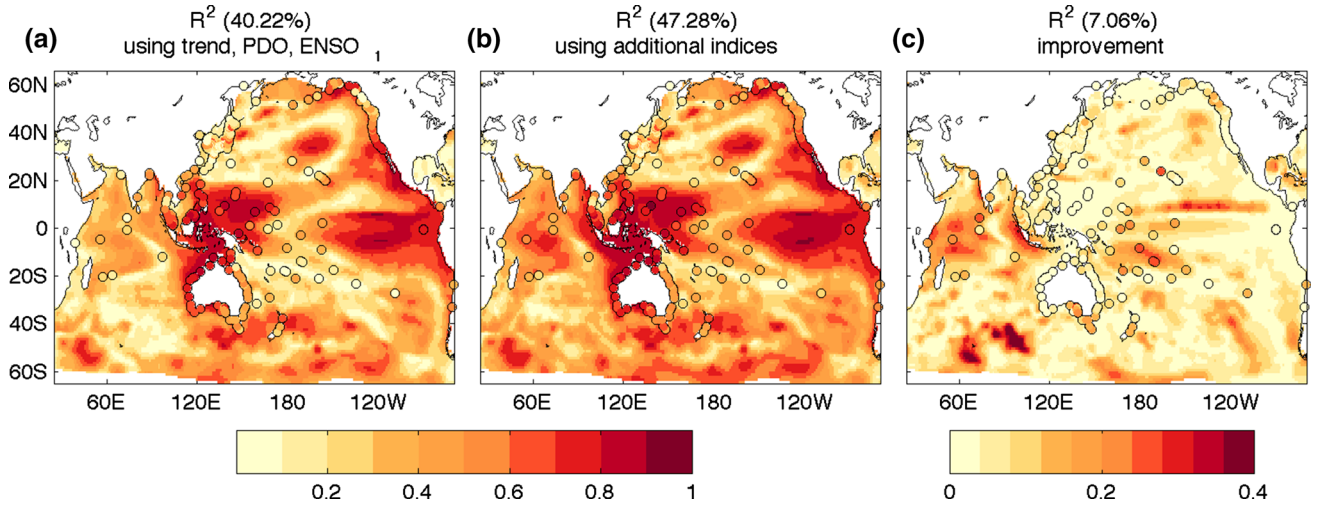

Fig. 4 R^2 values (variance explained by the regression divided by total variance) for altimetry and tide gauges from 1993 to 2007 for **a** regression including the residual trend, the PDO and $ENSO_1$, **b** regression including the residual trend, the PDO, two ENSO indices, the IOD and the SAM, and **c** the improvement achieved by including the extra indices

ENSO. This is supported by the fact that the correlations between the two ENSO indices and the IOD index (shown in Table 1) are the highest of all the indices used here. We can also see that the filtering used to separate the PDO and ENSO time scales is not perfect, since the overlap between the two is 2.78 out of a combined R^2 value of 36.07, however the correlations between the PDO and the ENSO indices are small. Similarly we can see that there is a small overlap between the PDO and the residual trend (2.01 out of a combined R^2 value of 30.00), while SAM and the residual trend seem to be largely independent (0.26 out of a combined R^2 value of 14.14). The overlap between the PDO and the trend is due to the presence of a trend in the PDO index over this time window, such that linear regression can not distinguish between the trend in SSH caused by the trend in the PDO and the trend in SSH due to other causes. Thus it remains to be seen whether these regression coefficients are robust to changes in window length and the period of observation.

Table 2 R^2 values (variance explained by the regression divided by total variance) for altimetry when different climate indices are included in the regression analysis

Indices	R^2 (%)
Trend	10.84
PDO	19.16
$ENSO_1$	14.87
$ENSO_2$	2.04
$ENSO_{1+2}$	16.80
PDO + $ENSO_{1+2}$	33.18
IOD	9.02
$ENSO_{1+2}$ + IOD	19.68
SAM	3.30
Residual trend + PDO	27.99
Residual trend + $ENSO_{1+2}$	27.76
Residual trend + IOD	19.56
Residual trend + SAM	13.88
Residual trend + PDO + $ENSO_{1+2}$	42.21
Residual trend + $ENSO_{1+2}$ + IOD	30.60
Residual trend + PDO + $ENSO_{1+2}$ + IOD + SAM	47.28

3.2 Robustness of regressions in time

The analyses of altimetric SSH is limited by the length of the altimetry record. Given that there is low frequency variability with a period longer than the available observations, we have to ask the question: does the short window length influence the amount of SSH variability and trend during the altimetry period that can be explained by the climate indices? For this reason we turn to two models, MOM0.25 and SODA to identify how robust (or stationary) the climate index regression patterns are to the 15-year period used in the calculation. Figure 5 shows R^2 values for altimetry compared to the two models. The three agree reasonably well in the equatorial regions, as may be expected due to the nature of the equatorial waveguide, as long as the tropical wind forcing is reasonably accurate in the two models. In contrast, the processes controlling sea level in the extratropics are more complex and atmospheric wind-forced variability is highly stochastic, requiring the models to be both correctly forced and accurate in their representation of the ocean circulation. This is reflected in the differences

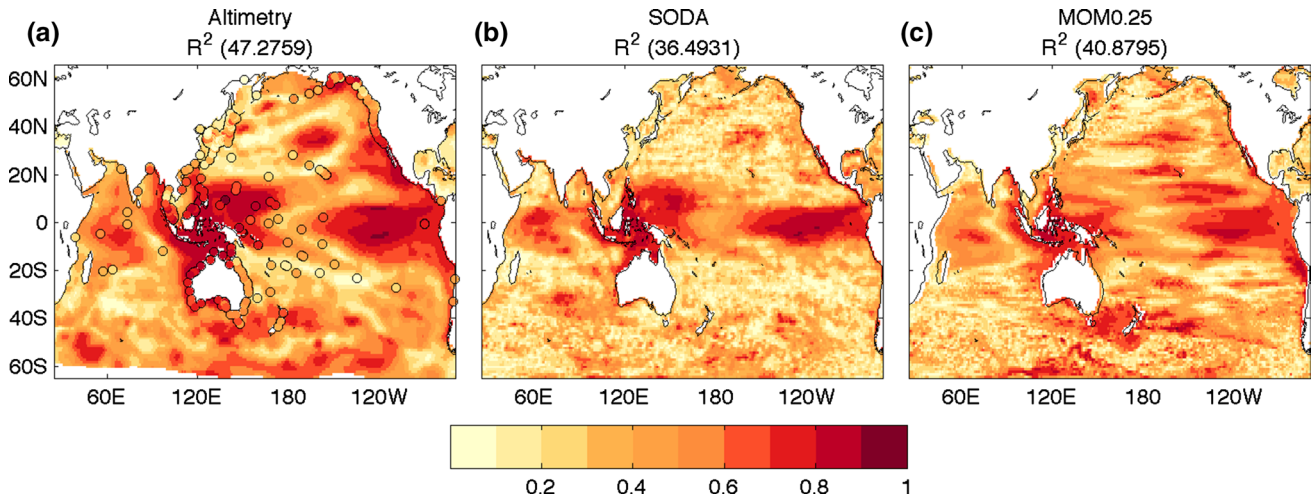

Fig. 5 R^2 values for a 15-year window (1993–2007) for different products **a** altimetry and tide gauges, **b** SODA and **c** MOM0.25

between altimetry and the two models in the extratropical regions in Fig. 5. For consistency with altimetry we calculate the regressions with observed indices rather than indices derived from the models themselves, which may introduce an additional error. The error is, however, expected to be small, due to the use of data assimilation in SODA and reanalysis surface winds and fluxes to force MOM0.25.

To test the robustness of the regression patterns in time we look at regression coefficients for SSH calculated for three different 15-year periods (1963–1977, 1978–1992 and 1993–2007) in the two models. Figures 6 and 7 show how the regression patterns change between the three different time windows. For the most recent period the patterns are similar to those obtained from altimetry for most of the indices (compare to Fig. 3), the largest differences being in the residual trend. Differences between altimetry and the models as well as differences between the two models may be explained by differences in the surface forcing used in each model, as suggested by Chepurin et al. (2014). In addition there may be differences in model physics as well as the impact of the hydrographic data which is assimilated into SODA. There are differences in the regressions calculated over the three periods in both the models. For most of the indices included in the regression calculation the earliest period (1963–1977) more closely resembles the later period (1993–2007) while the middle period (1978–1992) shows very little SSH variability related to $ENSO_2$ and the IOD in particular. The PDO-related SSH variability in the three periods looks quite different, with the later period closer to the earlier than the middle period, however the magnitude of the regressions is largest in the latest period. Residual SSH trends in the three periods are both large and inconsistent. Part of this inconsistency may be due to spurious model trends (related to incomplete spinup, for example), however the tide gauges also show similar differences in the residual trend patterns between periods, indicating that the model residual trends are at least partly due to observed climatic variability not represented by our selection of climate indices. There are also differences in the SSH regression on to the SAM, particularly in the equatorial Pacific, indicating that the equatorial Pacific SSH response to the SAM may not be robust. In general SODA shows lower R^2 values than MOM0.25. Both show R^2 values decreasing from the late 60s and early 70s before increasing again after the late 90s.

There are several reasons why the regressions may be different between the different periods:

1. *The window length is too short to fully capture/separate the modes of variability*. Short window length is most likely to be a problem when trying to distinguish between the trend and SSH anomalies due to low frequency variability such as the PDO (Lee and McPhaden 2008), where the period of the variability is longer than the window length. It should also be taken into consideration for ENSO and IOD-related SSH variability, since the two climate modes are not independent (Kug and Kang 2006; Santoso et al. 2012).
2. *The modes are not symmetric*. For example El Niño and La Niña are not mirror images of each other. Such nonlinearities are not captured by linear regression analysis, therefore if one time period contains more El Niño events then the regression coefficients will be different from another time period which contains more La Niña events. This may also be true for SSH regressions on to the PDO, for which the time series of observations is too short to robustly determine if the positive and negative PDO phases are symmetric or not.

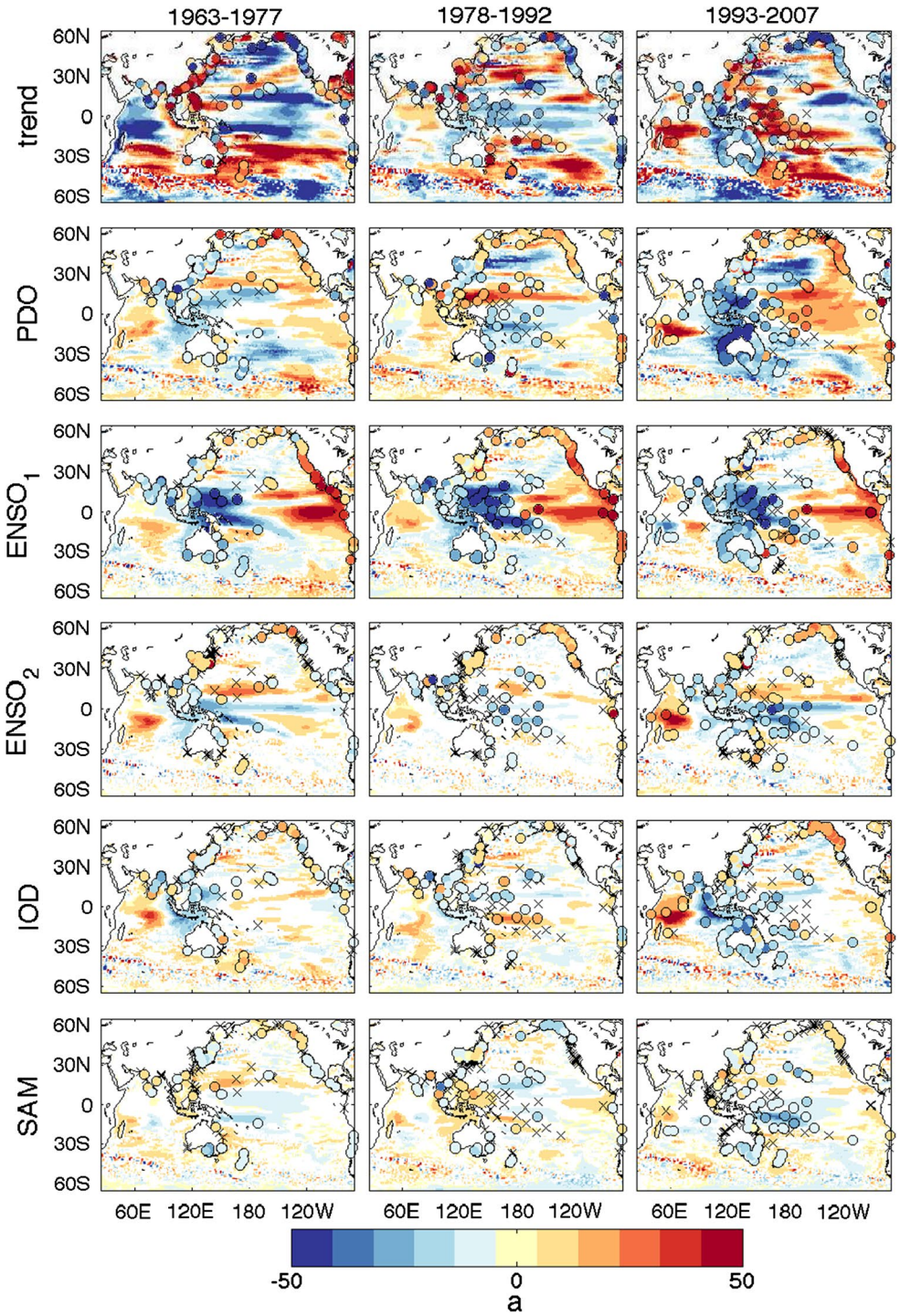

Fig. 6 Comparison of regressions with MOM0.25 for three different 15-year periods, 1963–1977 (*left column*), 1978–1992 (*middle column*) and 1993–2007 (*right column*) for the residual trend, PDO, two ENSO indices, IOD and SAM. Regression coefficients which are not significantly different from zero (at the 95 % level) are not shown. Regression coefficients for tide gauges in each period are shows as *coloured circles*. *Crosses* indicate tide gauges where data was available but the regressions were not significant

3. *Low frequency modulation of high frequency variability*. ENSO, for example, exhibits multi-decadal modulations in both amplitude and spatial pattern, some of which may be linked to the PDO (McGregor et al. 2010, 2013; Santoso et al. 2013; Wittenberg et al. 2014). Linear regression analysis is unable to capture this, and thus the regression coefficients of SSH with ENSO would appear to be different depending on the

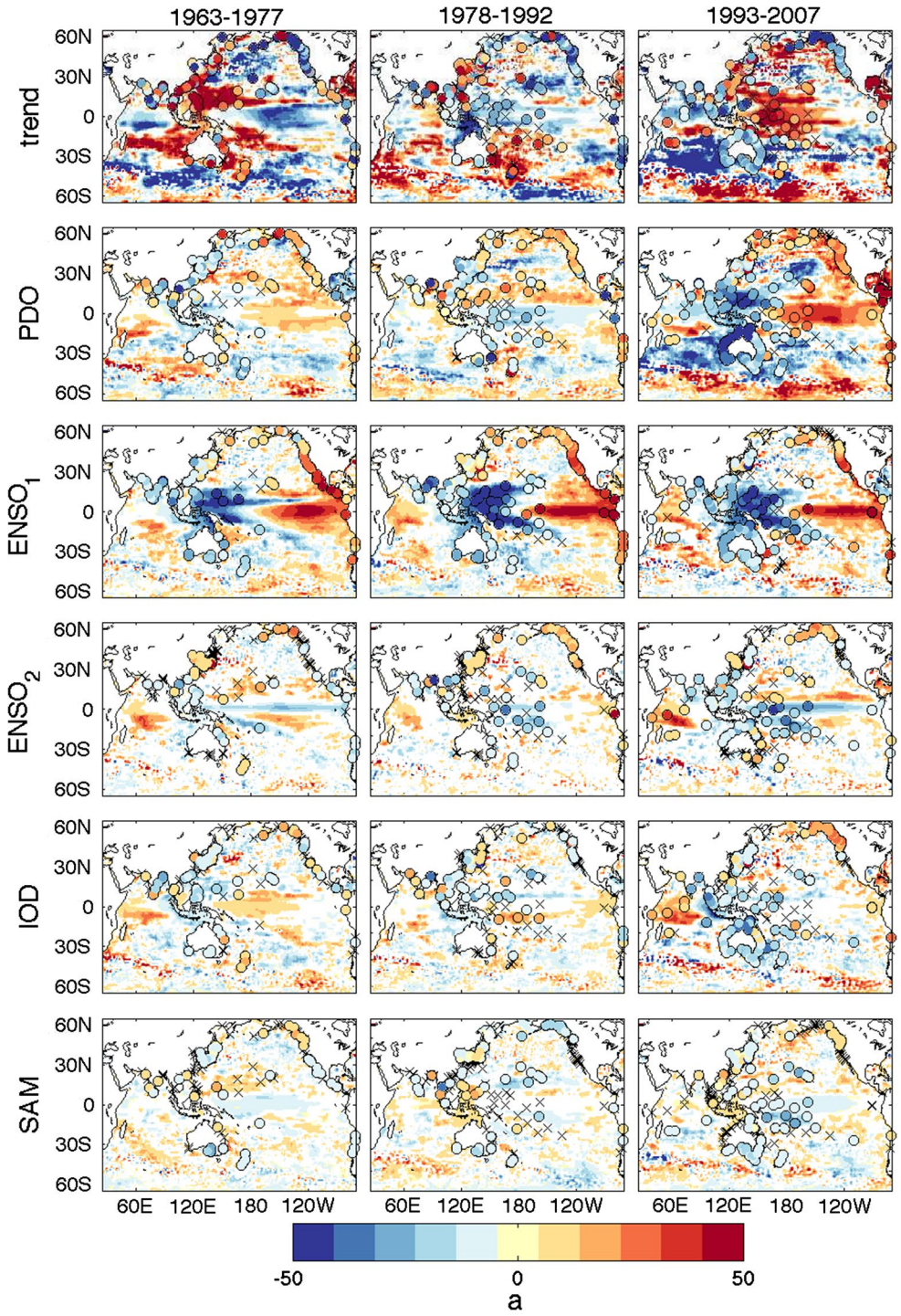

Fig. 7 As in Fig. 6 but for SODA

phase of the PDO. Low frequency modulation of the IOD and SAM would be similarly affected.

The apparent non-stationarity of the regression coefficients with time also applies to EOFs of SSH, such as those used in long reconstructions of sea level by Church and White (2011), Meyssignac et al. (2012a) and others. This limits the usefulness of these reconstructions outside of the altimetry period (as discussed by Calafat et al. 2014).

The analysis of the changes of regression coefficients may be extended to other time periods. Figure 8 shows Taylor diagrams (Taylor 2001) comparing the model regression

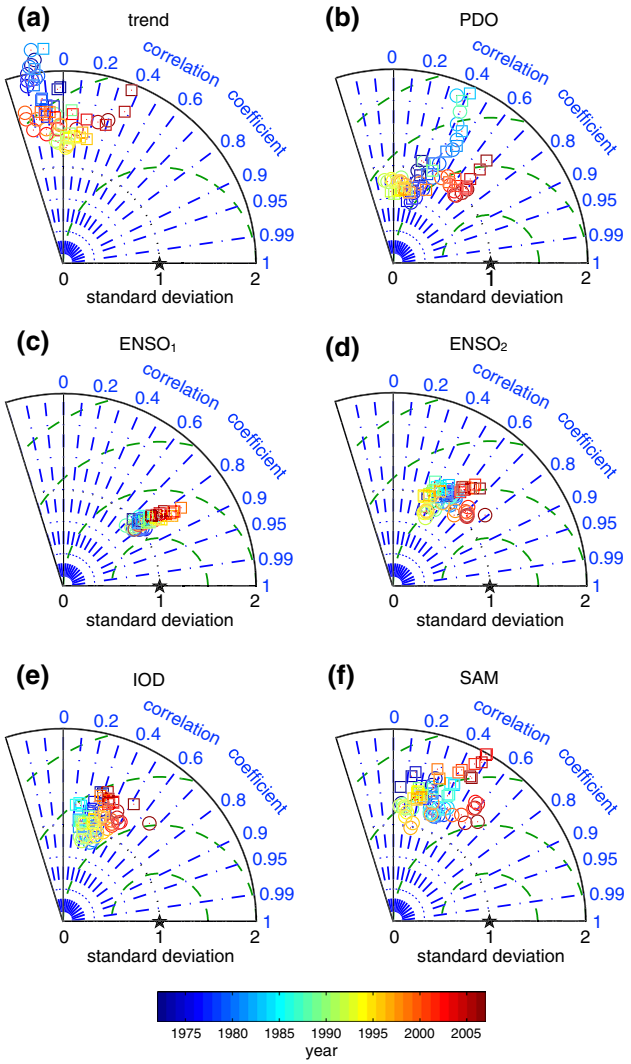

Fig. 8 Taylor diagrams of regression coefficients for different products and time periods compared to altimetry (represented by the *black star*) for the different climate indices. *Coloured symbols* represent overlapping 15-year windows, coloured by the last year of the window. *Squares* represent SODA and *circles* MOM0.25

coefficients to those derived from altimetry for the different regression terms for overlapping 15-year windows. The residual trends in the two models show low correlations and considerable spread compared to altimetry (Fig. 8a). Some of this spread can be attributed to processes which are not well represented by the models as well as to spurious model trends. A part of the spread, however, may be linked to incomplete separation of the trend and low frequency variability, which is confirmed by the large spread of points for the SSH regression on to the PDO (Fig. 8b). This spread indicates that a 15-year window is not long enough to properly capture the low frequency SSH variability and separate it from the trend. The inability to distinguish between trend and low frequency variability may be the reason that the 1993–2007 PDO-related SSH regression coefficients in Figs. 6 and 7 have larger variance than the earlier two periods. From Fig. 8b we can see that even higher variances were found for PDO-related SSH variability in the models from the late 1960s to the early 1980s. During these decades the PDO index displayed a significant trend (see Fig. 2b) which would be indistinguishable, in a short window, from the long term trend.

The highest correlations between models and altimetry occur for the first ENSO index (Fig. 8c), indicating that the models are doing a reasonable job of simulating SSH variability associated with ENSO and that the window length is long enough to capture that variability. Similarly the models appear to adequately capture the SSH variability associated with the second ENSO index (Fig. 8d).

Increased IOD variance (Abram et al. 2008) and a strengthening of (multi-) decadal equatorial Pacific SSH and wind variability (Han et al. 2013; England et al. 2014) have been observed during the late 20th Century. There is some hint of this change in IOD behaviour in Fig. 8e, where IOD-related SSH variance increases after the early 1990s. Correlations between both IOD and SAM-related SSH variability in altimetry and models remain low, however.

Comparing the behaviour of the two models we can see that both models have similar correlations with altimetry for ENSO, IOD and SAM-related SSH variability, although SODA (squares) has higher variance than MOM0.25 (circles). For the PDO-related SSH variability SODA and MOM0.25 agree with each other more closely during earlier periods, after the mid-1980s SODA shows higher variance.

3.3 Differences in wind products

Part of the differences between SODA and MOM0.25 can be explained by differences in the winds used to force the two models. SODA uses ERA-40 wind stresses from 1958 to 2001 and ERA-interim from 2002 to 2008 (Czeschel et al. 2011) while MOM0.25 uses corrected NCEP winds (Griffies et al. 2009). There have been several studies examining the differences between these (and other) wind products. Both McGregor et al. (2012a) and Nidheesh et al. (2013) found broad agreement between the wind products on interannual to decadal time scales but differences in longer term trends. These product differences were also highlighted by Wittenberg (2004), who found that wind stress anomalies are weaker and less noisy in NCEP than in ERA-40.

The influence of the different wind products used to force MOM0.25 and SODA can be estimated by comparing the response of a shallow water model (SWM) to each wind product. We use a linear shallow water model (1.5 layer reduced gravity model) in which the interface separating the upper and lower model layers represents the tropical

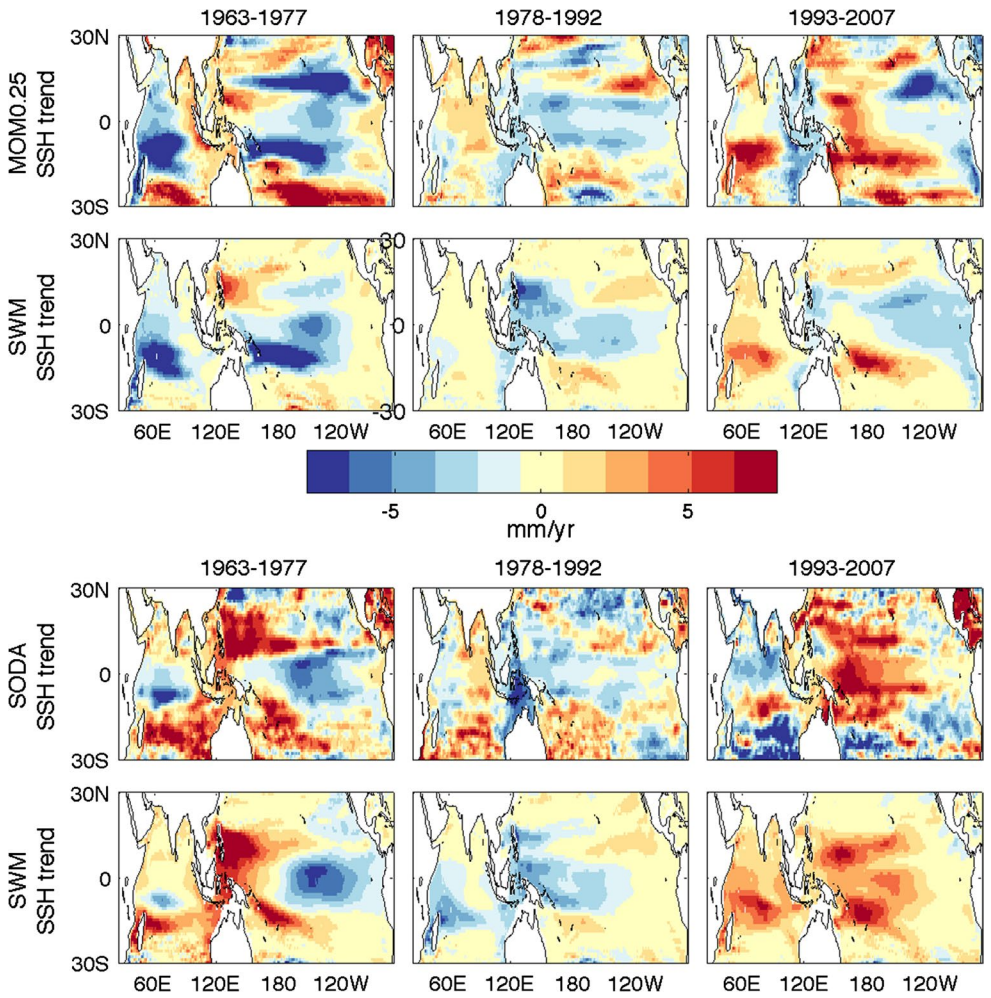

Fig. 9 Residual SSH trend (in mm/year) in three different time windows from MOM0.25 and from a shallow water model forced by the residual trend in the MOM0.25 winds (*upper panels*) and the same from SODA (*lower panels*)

thermocline. The thermocline depth is then translated into SSH using linear regression coefficients between modelled thermocline depth anomalies and observed SSH, as described by McGregor et al. (2012a). Shallow water models have already been used to study ENSO-related SSH variability (Timmermann et al. 2010; Widlansky et al. 2014) so we focus on the residual trend and PDO-related components of the wind. Figure 9 shows the results when the shallow water model is forced with the residual wind trend from three different periods from MOM0.25 and SODA, Fig. 10 shows the results for the PDO-related component of the wind. Only the area between 30°S and 30°N is plotted, since outside of this region the relationship between model thermocline depth and SSH is not robust (Timmermann et al. 2010). For both the residual trend and the PDO-related SSH variability, the shallow water model does a reasonable job of reproducing the large-scale patterns seen in the two models. Note that the SWM shows less small-scale SSH variability than the other two models, due to the fact that it is missing many of the processes which create variability on small scales. For this reason we focus on the large-scale SSH patterns associated with the various patterns of wind forcing, which the SWM is able to simulate. The ability of the SWM to reproduce the SSH patterns from SODA and MOM0.25 indicates that, when it comes to model differences in SSH patterns, data assimilation in SODA and model drift (in both models) may not be first order effects and that most of the trend and low frequency variability in SSH may in fact be due to the trend and low frequency variability in the wind. The SWM results thus suggest that a large part of the differences in trend and low frequency variability between the two models can be attributed to differences in the wind products used to force them.

3.4 Regressions over a longer time window

It is clear that a 15-year window is not long enough to reliably separate trend and low frequency variability. So how

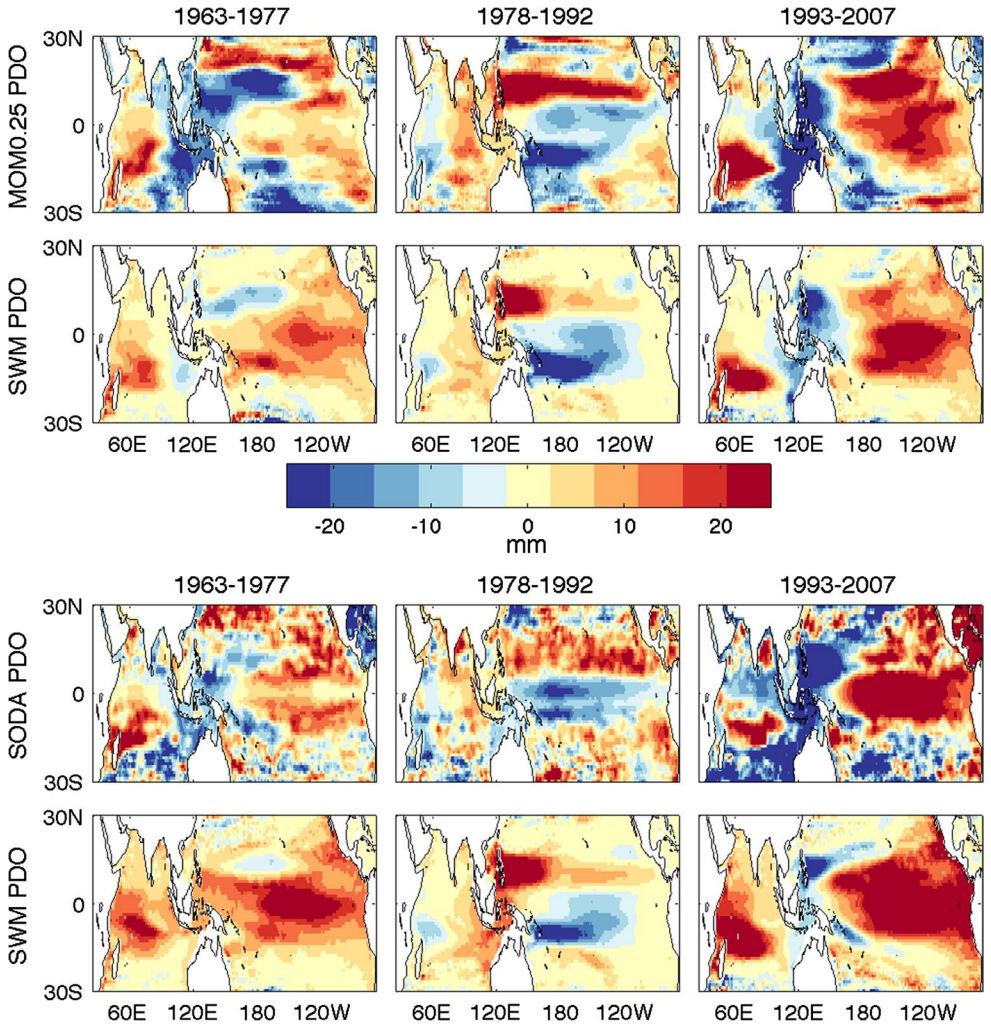

Fig. 10 SSH regressed on to the PDO index in three different time windows from MOM0.25 and from a shallow water model forced by the PDO winds (*upper panels*) and the same from SODA (*lower panels*)

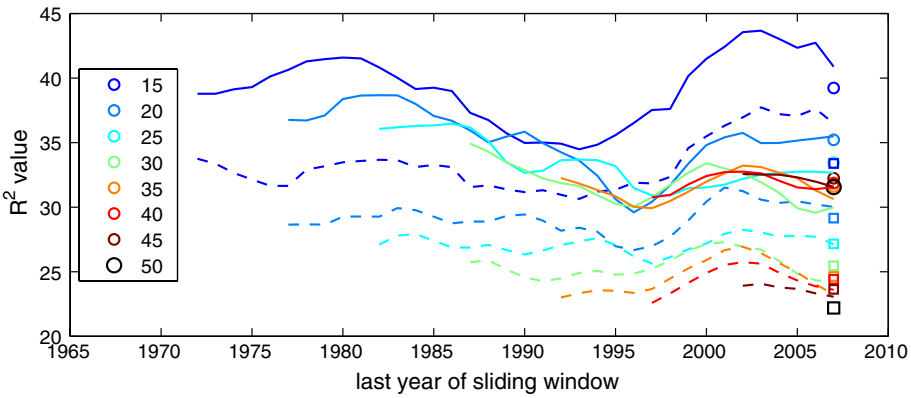

Fig. 11 R^2 values for window lengths from 15 to 45 years (*colours*) for MOM0.25 (*solid lines*) and SODA (*dashed lines*), plotted against the last year included in the sliding window. The average R^2 value for each window length is plotted as *circles* (for MOM0.25) and *squares* (for SODA) with the 50-year window plotted as a *black symbol*. Note that the *y-axis* does not start from zero

long does the window need to be? Figure 11 shows R^2 values averaged over the domain for a range of window lengths from 15 to 50 years for both MOM0.25 and SODA. As the window length increases the average R^2 values decrease, due to the fact that as the window length is increased there is a wider range of variability (i.e. more events) that must be explained by the regression coefficients, preventing the regression from overfitting to one particular event. Taking

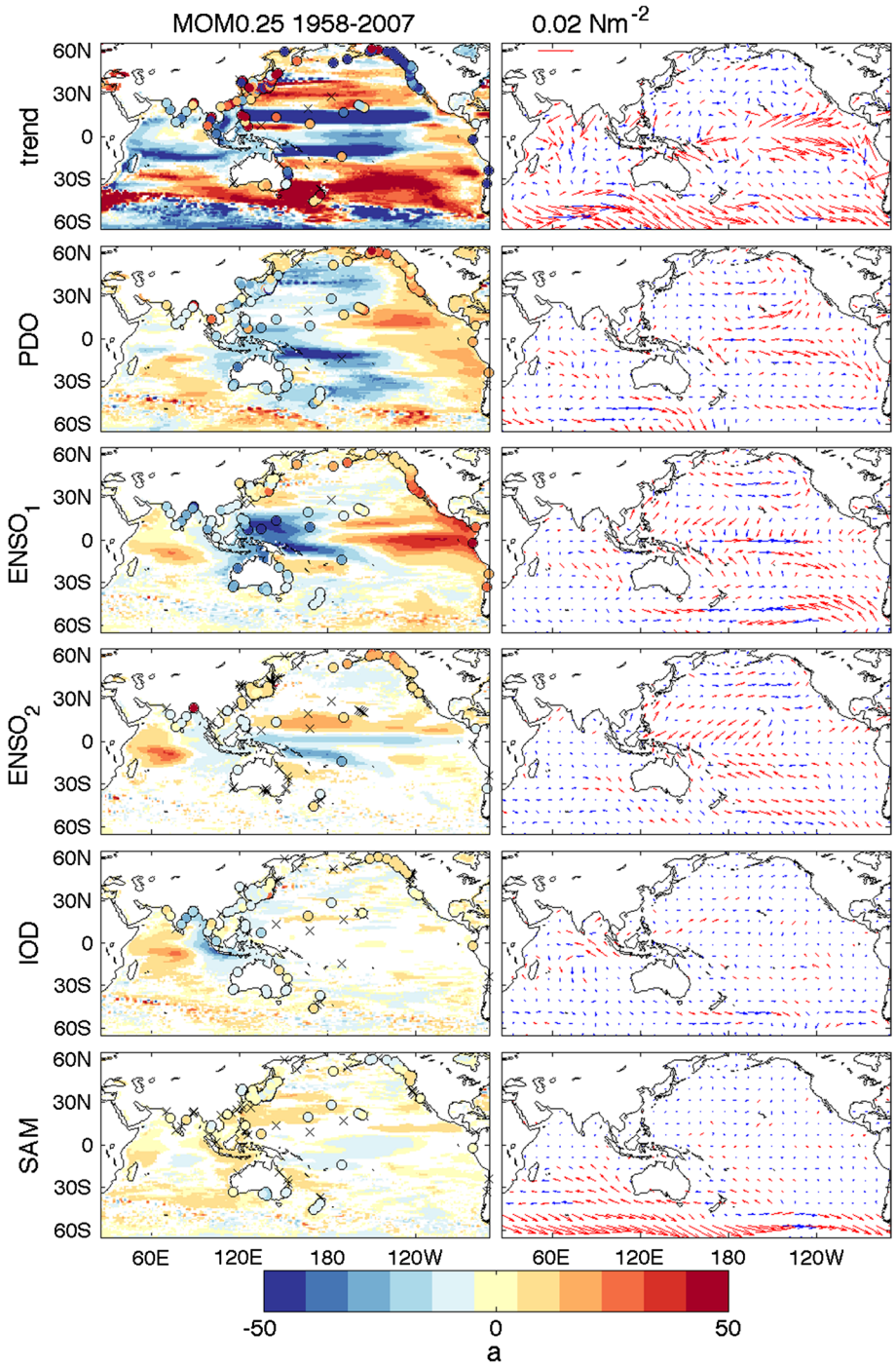

Fig. 12 Regression coefficients calculated using 50-years (1958–2007) of SSH (*left column*) and wind (*right column*) from MOM0.25. Tide gauges are shown as *coloured circles*, *crosses* indicate where the tide gauge regressions are not significant. Every eighth wind vector is plotted, *red vectors* indicate significance at the 95 % level

ENSO as an example, a short window which includes the large 1997–1998 El Niño will be able to describe that particular large event accurately. However, when the window is expanded to include other, smaller ENSO events (and La Niñas as well as El Niños) then the regression coefficients calculated over the shorter window may not be able to describe a particular individual event so well.

For MOM0.25 the R^2 values appear to be converging for window lengths above 30 years, but for SODA the R^2 values are still decreasing with increasing window length up to the maximum window length of 50 years. In the absence of a longer dataset to more thoroughly test convergence of the regressions, we will use the maximum window length of 50 years.

In addition to the change of average R^2 value with window length, Fig. 11 shows that there are particular years whose inclusion in the window have a marked effect on the R^2 value. The 15-year windows (dark blue curves) show

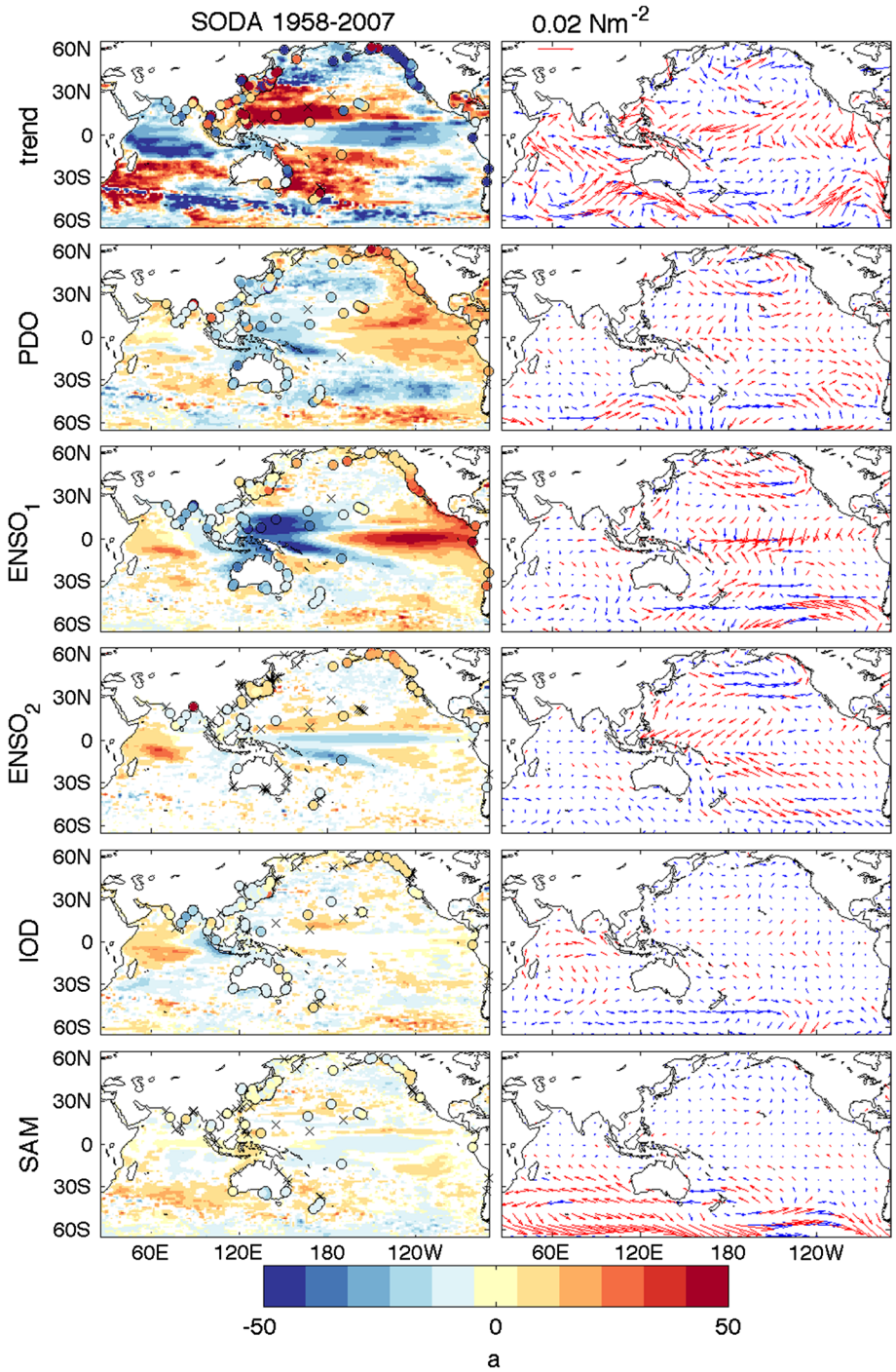

Fig. 13 As in Fig. 12 but for SODA

the largest R^2 values for windows ending in the early 2000s and around 1980 and the lowest values in windows ending in the early 1990s, which matches the results shown in Figs. 6 and 7. Windows ending in the early 2000s have the highest R^2 values across all window lengths, illustrating the importance of particular events/periods in influencing the regression patterns even for long window lengths.

In Figs. 12 and 13 we show regression coefficients calculated for both SSH and winds over a 50-year window (1958–2007) from MOM0.25 and SODA. For both models the regression patterns for $ENSO_2$, IOD and SAM-related SSH variability resemble those in 1993–2007 and 1963–1977. The PDO-related SSH pattern is also more similar to the 1993–2007 and 1963–1977 patterns than to the 1978–1992 pattern, but with smaller amplitudes than the 1993–2007 pattern. The models have quite different residual trend patterns (both to each other and to the residual trend patterns calculated over the shorter windows).

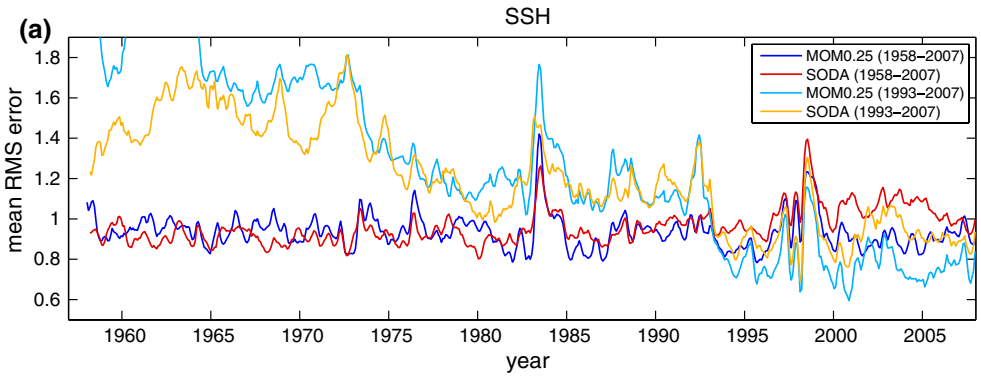

Fig. 14 RMS error for reconstructed **a** sea level and **b** wind stress curl using regression coefficients calculated over the 50-year window (*dark blue/red*) and the 1993–2007 window (*cyan/orange*) for MOM0.25 (*blue/cyan*) and SODA (*red/orange*). Note that the *y-axis* does not start from zero

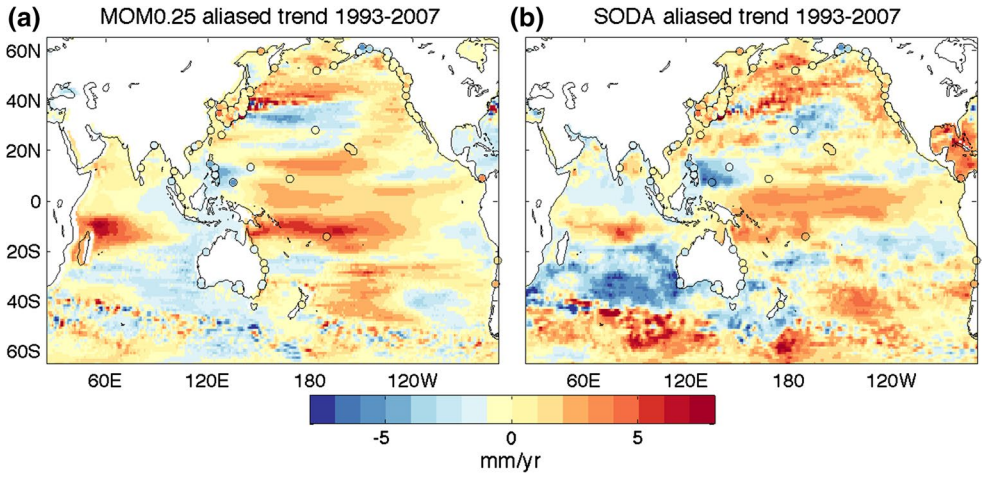

Fig. 15 SSH trend (in mm/year) over 1993–2007 attributed to the PDO when using a 15-year window rather than a 50-year window in (**a**) MOM0.25 and (**b**) SODA. Tide gauges are shown in *circles*

Figure 14a shows the skill of the regression at capturing the SSH variability in each model over both long and short windows. There are large spikes in the RMS error coinciding with the El Niño events of 1982–1983 and 1997–1998, indicating the inability of the linear regression to capture the nonlinear parts of the variability, which is particularly evident for large ENSO events. Regression coefficients calculated over the 15-year window 1993–2007 show lower errors when used to reconstruct SSH during that window, but large errors outside of it. The regression coefficients calculated using a 50-year window have a consistent level of skill at explaining the SSH variability in their respective models, at least until the last decade or so, when there is an increase in the RMS error for SODA. This increased error indicates that there has been a change in the model SSH variability such that the same set of regression coefficients cannot explain both pre- and post-2000s variability. The fact that a similar shift is not present in MOM0.25 indicates

that once again it may be due to the different wind products used by each model. Figure 14b shows that using regression coefficients to reconstruct the wind stress curl used in SODA undergoes a similar change in skill in the 2000s as the reconstructed SSH, indicating that the wind stress curl has undergone a similar shift. In particular, there appears to be a change in seasonality. The winds used in SODA have larger trends and low frequency variability towards the end of the model run compared to the MOM0.25 winds, which may be related to the switch from ERA-40 to ERA-interim in 2001 in SODA.

A large part of the error when calculating PDO-related SSH variations using a window that is too short is due to the false attribution of trends in the SSH to short term trends in the PDO index during the window. This false attribution is called trend aliasing. We can use the regression coefficients calculated using the 50-year window to find the aliasing that occurs during the 1993–2007 window in both SODA and MOM0.25, as shown in Fig. 15. This figure shows the part of the trend in SSH that is attributed to the PDO in the 15-year window, but which remains unexplained when using a more robust measure of the SSH regression on to the PDO (calculated over the 50-year window). This unexplained part of the trend could be due to either a trend in another climate index not included here (anthropogenic forcing, for example), or to a change in behaviour of the SSH regression on to the PDO during the recent period. A similar result was found by Han et al. (2013), who found that changes in the PDO/IPO cannot explain recent sea level rise in the western tropical Pacific and by England et al. (2014), who showed that the PDO/IPO only accounts for approximately half of the 1992–2011 acceleration in the trade winds. Instead, the large SSH changes in the tropical Pacific may have also been influenced by warming in the Indian (Han et al. 2013) and Atlantic (McGregor et al. 2014) Oceans.

4 Conclusions

Sea level variability during the 15-year altimeter period can be associated with various climate indices, such as the PDO, ENSO, IOD and SAM. Two ENSO indices, the first an ENSO index such as the MEI and the second representing the combination mode of ENSO and the annual cycle, can be used to explain more SSH variance in the central equatorial Pacific than the single ENSO index alone. The ENSO indices have significant regressions with SSH in the Indian Ocean, as does the IOD in the Pacific Ocean, indicating that ENSO and the IOD are not independent. However, the inclusion of the IOD explains more SSH variance in the Indian Ocean than ENSO alone. Regression of SSH with SAM does have a significant signal in the Southern Ocean as expected, however there are also signals of similar magnitude in the equatorial Indian and Pacific. It is likely, given the short length of the time series, that there is significant cross contamination between the low frequency variability and the trend, thus a longer time series is required to test the robustness of the SAM-related SSH signals.

Patterns of wind variability can also be associated with the climate indices. Using a shallow water model we find that a large part of the trend and low frequency variability of SSH in the SODA and MOM0.25 models can be explained by the trend and low frequency components of the wind forcing, suggesting that model drift is not a dominant factor. Some of the differences in SSH variability in SODA and MOM0.25 can be attributed to the different wind products used to force them. The MOM0.25 wind forcing has lower variance than the SODA wind forcing on all time scales and the two also exhibit significantly different 15-year residual trends, this difference between the two models is greatest in the most recent period.

Using the two models we can also test the robustness of the regression patterns to the length of the time series used to calculate them. Window lengths of 15 years appear to be sufficient for shorter period variability such as ENSO, however it is not sufficient for distinguishing between ENSO- and IOD-related SSH variability (which may in fact be impossible using this method due to the nonlinear nature of their interaction). Anomalously large events (such as the 1997–1998 El Niño) can still dominate due to overfitting when short window lengths are used, such that there is a dependence of the regressions on the time window chosen. The residual trend and the PDO-related SSH patterns are particularly sensitive to the length and position of the window. Indications are that a 15-year window is not enough to reliably separate the trend from the PDO-related SSH variability, which is reflected in the fact that $R2$ values for regressions calculated using 15-year windows were lower during the 1980s and 1990s than during the earlier and later periods. Window lengths on the order of 50 years (or longer) are required for robust regressions of SSH on to low frequency variability such as the PDO.

Comparing the amplitude of the regression of SSH on to the PDO during the altimetry record to the pattern and amplitude calculated over the 50-year window suggests that the more recent SSH–PDO relationship is not representative of the longer term record. This lack of robustness when using short window lengths also means that when estimating long term trends in spatial patterns of SSH (associated with anthropogenic climate change, for example) from the altimetry record we must take into account the fact that the patterns of 15-year trends vary considerably depending on the window and are influenced by low frequency modes of variability such as the PDO.

References

Abram NJ, Gagan MK, Cole JE, Hantoro WS, Mudelsee M (2008) Recent intensification of tropical climate variability in the Indian Ocean. Nat Geosci 1(12):849–853

Allan R, Ansell T (2006) A new globally complete monthly historical gridded mean sea level pressure dataset (HadSLP2): 1850–2004. J Clim 19(22):5816–5842

Cai W, Meyers G, Shi G (2005) Transmission of ENSO signal to the Indian Ocean. Geophys Res Lett 32(5):L05616

Calafat FM, Chambers DP, Tsimplis MN (2014) On the ability of global sea level reconstructions to determine trends and variability. J Geophys Res Oceans 119(3):1572–1592

Carton JA, Giese BS (2008) A reanalysis of ocean climate using Simple Ocean Data assimilation (SODA). Mon Weather Rev 136(8):2999–3017

Cazenave A, Dieng H-B, Meyssignac B, von Schuckmann K, Decharme B, Berthier E (2014) The rate of sea-level rise. Nat Clim Change 4(5):358–361

Chepurin GA, Carton JA, Leuliette E (2014) Sea level in ocean reanalyses and tide gauges. J Geophys Res Oceans 119(1):147–155

Church JA, Clark PU, Cazenave A, Gregory JM, Jevrejeva S, Levermann A, Merrifield MA, Milne GA, Nerem RS, Nunn PD, Payne AJ, Pfeffer WT, Stammer D, Unnikrishnan AS (2013) Sea level change. In: Stocker T, Qin D, Plattner G-K, Tignor M, Allen S, Boschung J, Nauels A, Xia Y, Bex V, Midgley P (eds) Climate change 2013: The Physical Science Basis. Contribution of Working Group I to the Fifth Assessment Report of the Intergovernmental Panel on Climate Change. Cambridge University Press, Cambridge

Church JA, White NJ (2011) Sea-level rise from the late 19th to the early 21st century. Surv Geophys 32(4–5):585–602

Czeschel R, Stramma L, Schwarzkopf FU, Giese BS, Funk A, Karstensen J (2011) Middepth circulation of the eastern tropical South Pacific and its link to the oxygen minimum zone. J Geophys Res Oceans 116(C1):C01015

Delworth TL, Rosati A, Anderson W, Adcroft AJ, Balaji V, Benson R, Dixon K, Griffies SM, Lee H-C, Pacanowski RC, Vecchi GA, Wittenberg AT, Zeng F, Zhang R (2012) Simulated climate and climate change in the GFDL CM2.5 high-resolution coupled climate model. J Clim 25(8):2755–2781

Ding Q, Steig EJ, Battisti DS, Wallace JM (2012) Influence of the tropics on the Southern Annular Mode. J Clim 25(18):6330–6348

Enfield DB, Allen JS (1980) On the structure and dynamics of monthly mean sea level anomalies along the Pacific coast of North and South America. J Phys Oceanogr 10(4):557–578

England MH, McGregor S, Spence P, Meehl GA, Timmermann A, Cai W, Gupta AS, McPhaden MJ, Purich A, Santoso A (2014) Recent intensification of wind-driven circulation in the Pacific and the ongoing warming hiatus. Nat Clim Change 4(3):222–227

Feng M, Li Y, Meyers G (2004) Multidecadal variations of Fremantle sea level: footprint of climate variability in the tropical Pacific. Geophys Res Lett 31(16):L16302

Folland CK, Renwick JA, Salinger MJ, Mullan AB (2002) Relative influences of the interdecadal Pacific oscillation and ENSO on the South Pacific convergence zone. Geophys Res Lett 29(13):1643

Frankcombe LM, Spence P, Hogg AM, England MH, Griffies SM (2013) Sea level changes forced by Southern Ocean winds. Geophys Res Lett 40(21):5710–5715

Griffies SM (2012) Elements of the Modular Ocean Model (MOM): 2012 release (GFDL Ocean Group technical report No. 7. GFDL Ocean Group technical report No. 7. NOAA/Geophysical Fluid Dynamics Laboratory, Princeton, USA

Griffies SM, Biastoch A, Böning C et al (2009) Coordinated ocean–ice reference experiments (COREs). Ocean Model 26(1–2):1–46

Griffies SM, Yin J, Durack PJ, Goddard P et al (2014) An assessment of global and regional sea level for years 1993–2007 in a suite of interannual CORE-II simulations. Ocean Model 78:35–89

Han W, Meehl G, Hu A, Alexander M, Yamagata T, Yuan D, Ishii M, Pegion P, Zheng J, Hamlington B, Quan X-W, Leben R (2013) Intensification of decadal and multi-decadal sea level variability in the western tropical Pacific during recent decades. Clim Dynam 1–23

Kleeman R, McCreary J, Klinger BA (1999) A mechanism for generating ENSO decadal variability. Geophys Res Lett 26(12):1743–1746

Kug J-S, Kang I-S (2006) Interactive feedback between ENSO and the Indian Ocean. J Clim 19(9):1784–1801

Lee T, McPhaden MJ (2008) Decadal phase change in large-scale sea level and winds in the Indo-Pacific region at the end of the 20th century. Geophys Res Lett 35(1):L01605

Mann ME, Steinman BA, Miller SK (2014) On forced temperature changes, internal variability and the AMO. Geophys Res Lett 41:3211–3219

Mantua NJ, Hare SR, Zhang Y, Wallace JM, Francis RC (1997) A Pacific interdecadal climate oscillation with impacts on salmon production. Bull Am Meteorol Soc 78(6):1069–1079

Marshall GJ (2003) Trends in the southern annular mode from observations and reanalyses. J Clim 16(24):4134–4143

McGregor S, Gupta AS, England MH (2012a) Constraining wind stress products with sea surface height observations and implications for Pacific Ocean sea level trend attribution. J Clim 25(23):8164–8176

McGregor S, Timmermann A, Schneider N, Stuecker MF, England MH (2012b) The effect of the south Pacific convergence zone on the termination of El Niño events and the meridional asymmetry of ENSO. J Clim 25:5566–5586

McGregor S, Timmermann A, England MH, Timm OE, Wittenberg AT (2013) Inferred changes in El Niño-southern oscillation variance over the past six centuries. Clim Past 9(5):2269–2284

McGregor S, Timmermann A, Stuecker MF, England MH, Merrifield M, Jin F-F, Chikamoto Y (2014) Recent walker circulation strengthening and Pacific cooling amplified by Atlantic warming. Nat Clim Change 4(10):888–892

McGregor S, Timmermann A, Timm O (2010) A unified proxy for ENSO and PDO variability since 1650. Clim Past 6(1):1–17

Meinen CS, McPhaden MJ (2000) Observations of warm water volume changes in the equatorial Pacific and their relationship to El Niño and La Niña. J Clim 13:3551–3559

Merrifield MA, Thompson PR, Lander M (2012) Multidecadal sea level anomalies and trends in the western tropical Pacific. Geophys Res Lett 39(13):L13602

Meyssignac B, Becker M, Llovel W, Cazenave A (2012b) An assessment of two-dimensional past sea level reconstructions over 1950–2009 based on tide-gauge data and different input sea level grids. Surv Geophys 33(5):945–972

Meyssignac B, Salas y Melia D, Becker M, Llovel W, Cazenave A (2012a) Tropical Pacific spatial trend patterns in observed sea level: internal variability and/or anthropogenic signature? Clim Past 8(2):787–802

Newman M, Compo GP, Alexander MA (2003) ENSO-forced variability of the Pacific decadal oscillation. J Clim 16(23):3853–3857

Nidheesh AG, Lengaigne M, Vialard J, Unnikrishnan AS, Dayan H (2013) Decadal and long-term sea level variability in the tropical Indo-Pacific Ocean. Clim Dynam 41:381–402

Peltier WR (2004) Global glacial isostasy and the surface of the ice-age earth: the ICE-5G (VM2) model and GRACE. Annu Rev Earth Planet Sci 32:111

Perrette M, Landerer F, Riva R, Frieler K, Meinshausen M (2013) A scaling approach to project regional sea level rise and its uncertainties. Earth Syst Dynam 4(1):11–29

Power S, Tseitkin F, Mehta V, Lavery B, Torok S, Holbrook N (1999) Decadal climate variability in Australia during the twentieth century. Int J Climatol 19(2):169–184

Qiu B, Chen S (2006) Decadal variability in the large-scale sea surface height field of the South Pacific Ocean: observations and causes. J Phys Oceanogr 36(9):1751–1762

Qiu B, Chen S (2012) Multidecadal sea level and gyre circulation variability in the northwestern tropical Pacific Ocean. J Phys Oceanogr 42(1):193–206

Ray RD, Douglas BC (2011) Experiments in reconstructing twentieth-century sea levels. Prog Oceanogr 91(4):496–515

Roemmich D, Gilson J, Davis R, Sutton P, Wijffels S, Riser S (2007) Decadal spinup of the South Pacific subtropical gyre. J Phys Oceanogr 37(2):162–173

Saji NH, Goswami BN, Vinayachandran PN, Yamagata T (1999) A dipole mode in the tropical Indian Ocean. Nature 401(6751):360–363

Santoso A, England MH, Cai W (2012) Impact of Indo-Pacific feedback interactions on ENSO dynamics diagnosed using ensemble climate simulations. J Clim 25(21):7743–7763

Santoso A, McGregor S, Jin F-F, Cai W, England MH, An S-I, McPhaden MJ, Guilyardi E (2013) Late-twentieth-century emergence of the El Niño propagation asymmetry and future projections. Nature 504:126–130

Slangen ABA, Katsman CA, Wal RSW, Vermeersen LLA, Riva REM (2012) Towards regional projections of twenty-first century sea-level change based on IPCC SRES scenarios. Clim Dynam 38(5–6):1191–1209

Spence P, Griffies SM, England MH, Hogg AM, Saenko OA, Jourdain NC (2014) Rapid subsurface warming and circulation changes of Antarctic coastal waters by poleward shifting winds. Geophys Res Lett 41:4601–4610

Stuecker MF, Timmermann A, Jin F-F, McGregor S, Ren H-L (2013) A combination mode of the annual cycle and the El Niño/Southern Oscillation. Nat Geosci 6(7):540–544

Taylor KE (2001) Summarizing multiple aspects of model performance in a single diagram. J Geophys Res Atmos 106(D7):7183–7192

Timmermann A, McGregor S, Jin F-F (2010) Wind effects on past and future regional sea level trends in the southern Indo-Pacific. J Clim 23(16):4429–4437

Widlansky MJ, Timmermann A, McGregor S, Stuecker MF, Cai W (2014) An interhemispheric tropical sea level seesaw due to El Niño Taimasa. J Clim 27(3):1070–1081

Wittenberg AT (2004) Extended wind stress analyses for ENSO. J Clim 17:2536–2540

Wittenberg AT, Rosati A, Delworth TL, Vecchi GA, Zeng F (2014) ENSO modulation: Is it decadally predictable? J Clim 27(7):2667–2681

Wolter K, Timlin MS (2011) El Niño/Southern Oscillation behaviour since 1871 as diagnosed in an extended multivariate ENSO index (MEI.ext). Int J Climatol 31(7):1074–1087

Zhang X, Church JA (2012) Sea level trends, interannual and decadal variability in the Pacific Ocean. Geophys Res Lett 39(21):L21701